Photoconductivity of liquid crystalline derivatives of pyrene and carbazole†

Monika J. Sienkowska,[a] Hirosato Monobe,[b] Piotr Kaszynski*[a] and Yo Shimizu[b]

Received 25th August 2006, Accepted 11th December 2006
First published as an Advance Article on the web 15th January 2007
DOI: 10.1039/b612253a

Two structurally related discogens containing either pyrene (**1a**) or carbazole (**2a**) were investigated by thermal, XRD, spectroscopic, and time-of-flight (TOF) methods. Experiments demonstrated for **1a** a narrow range Col_h phase, which easily forms a glass state at ambient temperature. TOF measurements showed an ambipolar charge transport for **1a** with the mobilities on the order of 10^{-3} cm^2 V^{-1} s^{-1}. The carbazole **2a** has two enantiotropic phases (Cr_{col} and Col_h) and behaves as a p-type semiconductor. The activation energy for positive charge mobility in **1a** was found to be 0.10 $\pm$ 0.01 eV.

Introduction

Photogeneration of an electron–hole pair and one dimensional charge transport[1–8] along the self-assembled columns in aromatic discotic liquid crystals[9,10] has been recognized as an attractive property for construction of light emitting diodes,[11] photovoltaic cells,[12] and field-effect transistors.[13,14] The initial focus was on triphenylene-based discotics,[1] however other classes of discotics, including perylenes,[15] phthalocyanines,[16,17] hexabenzocoronenes,[18] and other polycyclic aromatics,[19] have been recently investigated for their photophysical properties. Typical charge mobility in these systems has been found to be in the range of 10^{-4}–10^{-1} cm^2 V^{-1} s^{-1},[9,20] which is comparable with those of polycrystalline organics[21,22] and attractive for device applications. In this context, we set out to investigate the photophysical behavior of discotic derivatives of pyrene and carbazole.

Photoconductive properties of pyrene were investigated in pure crystals,[23] in thin films,[24] and also in solutions of liquid hydrocarbons.[25] Carbazole derivatives are attractive for technological applications and they have been intensively studied in polymers[26–29] and as components of a discotic triphenylene derivative.[30] To date, no photoconduction studies of discotic liquid crystals solely based on pyrene or carbazole have been reported.

Recently, we prepared discotic derivative of pyrene **1a**.[31] Here, we report the preparation of the carbazole analog **2a**, and also XRD phase characterization and photoconductive properties of both pyrene and carbazole discotics **1a** and **2a**, which contain four 3,4-dioctyloxyphenyl substituents each. For comparison with other structurally similar discotics,[31] we also prepared and characterized carbazole derivatives **2b** and **2c**.

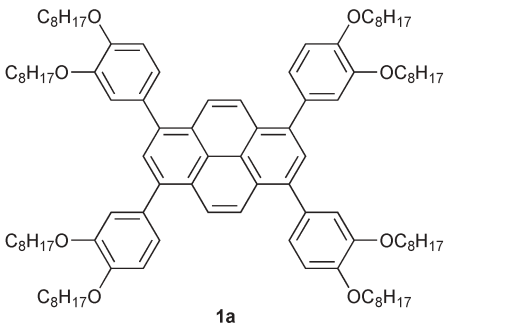

1a

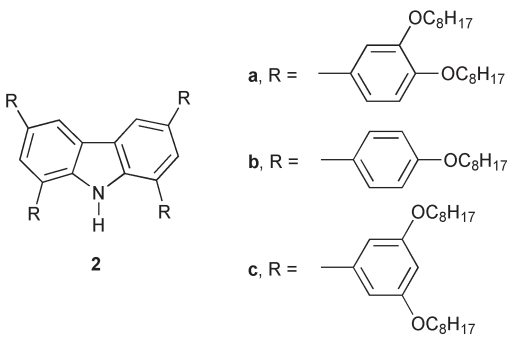

2

Results and discussion

Synthesis

Tetraarylcarbazoles **2** were prepared from 1,3,6,8-tetrabromocarbazole[32] (**3**) and appropriate boronic esters **4** according to the general Suzuki coupling procedure[33] (Scheme 1). Biphenyls **5** were obtained as the homocoupling byproducts. The

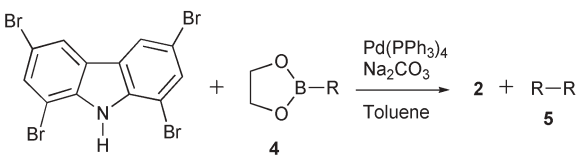

3 **4** **5**

Scheme 1

[a]*Organic Materials Research Group Department of Chemistry, Vanderbilt University, Nashville, TN, 37235, USA*
[b]*Nanotechnology Research Institute, National Institute of Advanced Industrial Science and Technology, AIST Kansai Centre, Midorigaoka 1-8-31, Ikeda, Osaka, 536-8577, Japan*

† Electronic supplementary information (ESI) available: UV, XRD, and photoconductivity data. See DOI: 10.1039/b612253a

desired tetraarylated carbazoles **2** were separated by column chromatography from partially arylated arenes and biphenyls **5** using a gradient polarity eluent. Chromatographic purification of **2a** and **2b** was followed by recrystallization from a hexane–ethanol mixture. Derivative **2c** was found to be an isotropic liquid at room temperature. Tetrabromide **3** was obtained by direct bromination of the parent carbazole according to a literature procedure.[32,34] Preparation of boronic esters **4**, characterization of biphenyls **5**, and preparation of pyrene derivative **1a** are described elsewhere.[31]

Liquid crystalline properties

The investigation of carbazoles **2a–2c** using polarized optical microscopy and differential scanning calorimetry (DSC) showed that only **2a** forms a liquid crystalline phase. Compound **2b** showed only melting to an isotropic phase upon heating at 114 °C (38 kJ mol^{-1}) and crystallization upon cooling, and derivative **2c** is an isotropic liquid at ambient temperature. These results are consistent with the observed behavior of pyrene and other analogs of **2**.[31] For instance, the benzo[*c*]cinnoline analog of **2c** was also found to exist as an isotropic liquid at ambient temperature. This was ascribed to the poor core–core interactions resulting from steric hindrance of the 3,5-dioctyloxyphenyl substituent.[31]

The mesophases obtained on cooling of compounds **1a** and **2a** displayed fan-shaped textures that are characteristic for columnar mesophases[35,36] (Fig. 1). The texture for **1a** was highly birefringent. In contrast, carbazole derivative **2a** showed large homeotropic domains with discotic columnar axes oriented perpendicular to the substrate in both liquid crystalline and crystalline phases. These textures remained virtually the same after cooling to room temperature.

Pyrene derivative **1a** melts to a discotic hexagonal phase at 73 °C, which is followed by isotropization at 87 °C (Fig. 2a).[31] On cooling, the isotropic–discotic transition is supercooled by 8 °C and no crystallization peak is observed at a scanning rate of 10 °C min^{-1}. The optical texture remained practically unchanged indicating the formation of an oriented glass at room temperature. This was confirmed by an attempt to shear the cover slip.

The DSC trace for carbazole derivative **2a** exhibits three transitions (Fig. 2b). The first endotherm at 60 °C with a small enthalpy of 3 kJ mol^{-1} was assigned as a transition to a crystalline columnar phase (Cr_{col}) as identified by XRD (*vide infra*). This was followed by melting to a hexagonal columnar mesophase at 109 °C and isotropization at 126 °C with an enthalpy of 20 kJ mol^{-1}. The cooling trace showed all three transitions progressively shifted to lower temperatures as the viscosity of the phases increased. Thus, the lowest transition temperature was supercooled by 16 °C. The second heating curve reproduced the transitions obtained for the virgin sample.

The formation of the crystalline columnar phase by **2a** and glassification of the Col_h in **1a** are consistent with observations for other discogens with the ''pinwheel'' substitution patterns and are desired for opto-electronic applications.[37–39] This can be rationalized by the relatively large core–core distance in the mesophase (*vide infra*) and consequently ineffective π–π interactions which typically drive the crystallization and molecular tilting of small aromatics.[40]

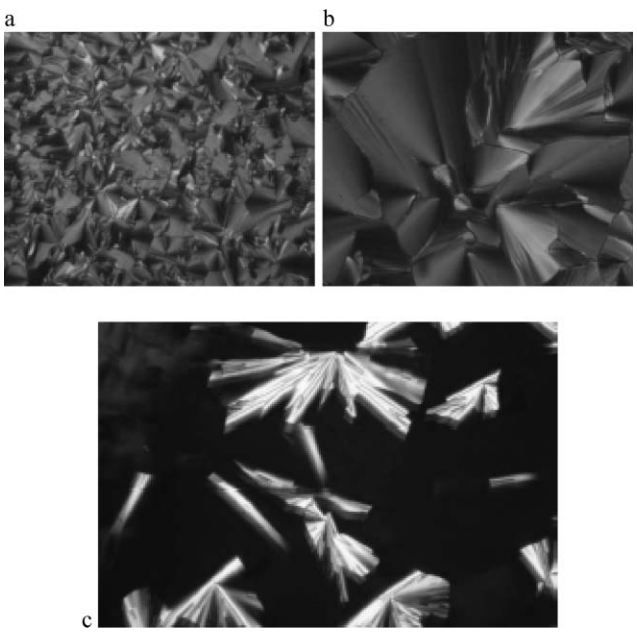

Fig. 1 Optical textures of (a) discotic hexagonal phase of **1a** at 75 °C (magnification 60×), (b) glass phase, retaining structural features of the preceding hexagonal mesophase of **1a** at room temperature (magnification 300×), (c) crystalline columnar phase of **2a** at 80 °C; the texture is identical with that of the discotic hexagonal phase obtained at higher temperature (magnification 300×).

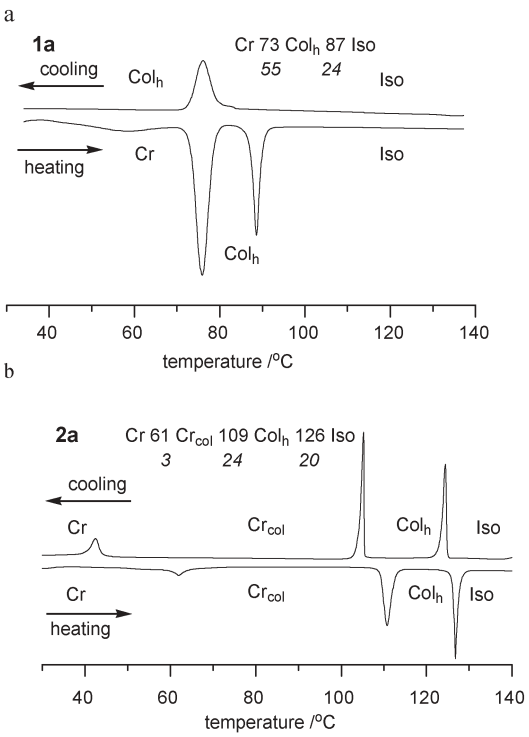

Fig. 2 DSC traces of a) pyrene **1a** and b) carbazole **2a**. Heating rate 10 °C min^{-1}. Transition temperatures (°C) and enthalpies (in italics, kJ mol^{-1}): Cr = crystalline, Cr_{col} = crystalline columnar, Col_h = hexagonal columnar, Iso = isotropic.

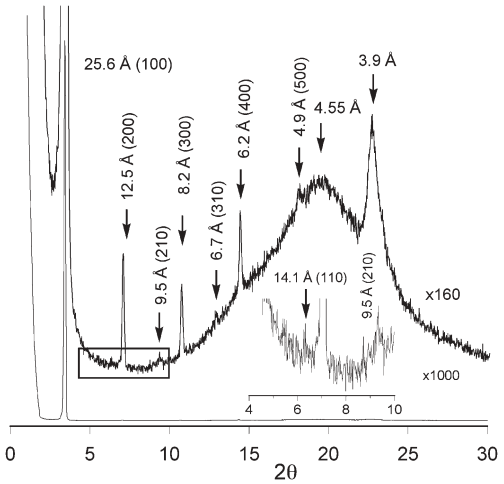

Fig. 3 XRD pattern for the Col_h mesophase of **1a** at 80 °C obtained by cooling from the isotropic phase. The boxed region is expanded in the inset.

Powder X-ray diffraction (XRD)

Liquid crystalline derivatives **1a** and **2a** were investigated by variable temperature powder X-ray diffraction to determine their phase structure. The results are shown in Fig. 3 and 4 and tabularized data is provided in the ESI.† The cell parameter *a* was calculated to be 28.9 Å for **1a** and 29.8 Å for **2a** using eqn (1) and assuming a hexagonal columnar mesophase structure for both compounds. The cell parameter *a* is smaller than the van der Waals diameter of the molecule (37 Å) in the most extended conformation. This indicates either interdigitation or partial folding of the chains in both **1a** and **2a**.

$$a = d_{200} \times 4 \Big/ \sqrt{3} \quad (1)$$

Diffractograms obtained for both compounds in the temperature regions identified to be liquid crystalline (*vide supra*) showed reflection patterns that can be ascribed to a two-dimensional hexagonal lattice of a columnar discotic liquid crystal.[41] Graphs of one-dimensional intensity as a function of the diffraction angle 2θ show the strong (100) peak and weak higher-order reflections (*hk*0) in the approximate spacing ratio of $d_{100}/\sqrt{3}$, $d_{100}/\sqrt{4}$, $d_{100}/\sqrt{7}$, *etc*. (Fig. 3 and 4a). For both compounds the (110) peak is surprisingly weak albeit detectable, and together with the more intense (210) and (310) reflections support the phase assignment to columnar hexagonal (Col_h). Both diffractograms are dominated by the (*h*00) reflections, with the (200) reflection being the second strongest. This rather unusual diffraction pattern observed for both compounds may result from incomplete powder averaging and, in consequence, unreliable relative intensities of the reflections.

The wide-angle region of the diffractograms shows a broad halo at around 4.6 Å indicating the mean distance between the molten alkyl chains within one column. The peak on the right side of the diffused feature arises from the core–core correlation. For **1a** the core-core mean distance is 3.9 Å at 80 °C, which is larger than the 3.7 Å measured for **2a** at 120 °C, both in the Col_h phase. Both of these values are larger than a typical 3.5 Å mean core–core separation in other discotics.[41]

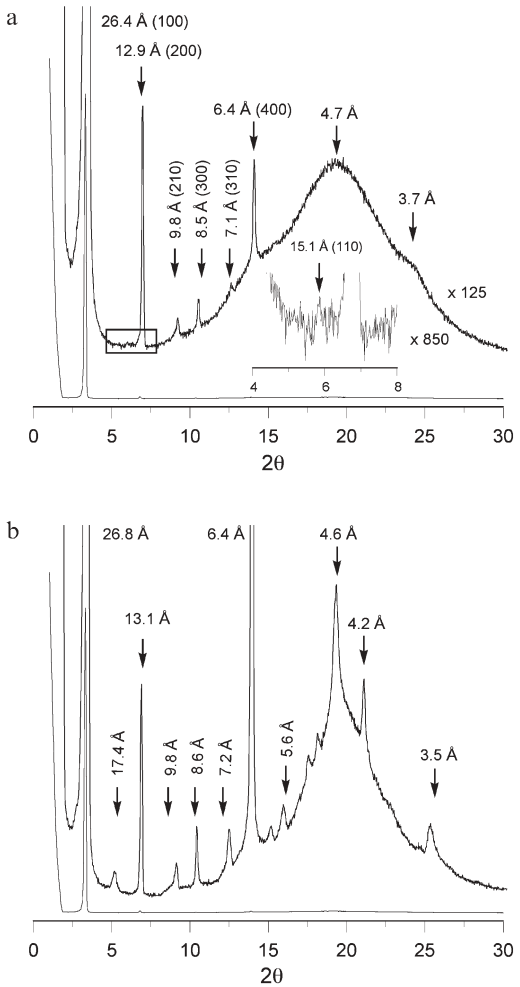

Fig. 4 XRD patterns for **2a**: a) a Col_h phase at 120 °C, and b) a Cr_{col} phase at 70 °C obtained by cooling from the isotropic phase. The boxed region is shown expanded in the inset.

A comparison of results obtained for carbazole **2a** at 120 °C and 70 °C shows similar X-ray diffraction patterns in the low angle, but significant differences in the wide-angle areas (Fig. 4). The wide-angle X-ray pattern for the hexagonal columnar mesophase at 120 °C shows only the broad halo, while the pattern at 70 °C displays additional sharp reflections in the range of 4.2 Å–5.9 Å. Thus, the X-ray diffraction pattern recorded at 70 °C appears to arise from periodic arrangement of molecules within each column, incorporating column-to-column registry, *i.e.* a three-dimensional crystal. However, alkyl chains in this phase are still significantly disordered, as indicated by the broad halo at about 4.5 Å. This pattern can be tentatively assigned to a crystalline columnar phase (Cr_{col}) based on the fact that the phase is formed upon cooling of the Col_h mesophase with unnoticeable texture change (*vide supra*).

Absorption spectroscopy

The UV absorption spectra for pyrene **1a** and carbazole **2a** derivatives in cyclohexane are shown in Fig. 5. Substitution of the parent carbazole with four 3,4-dioctyloxyphenyl groups results in a red-shift of its lowest energy transition by 33 nm to

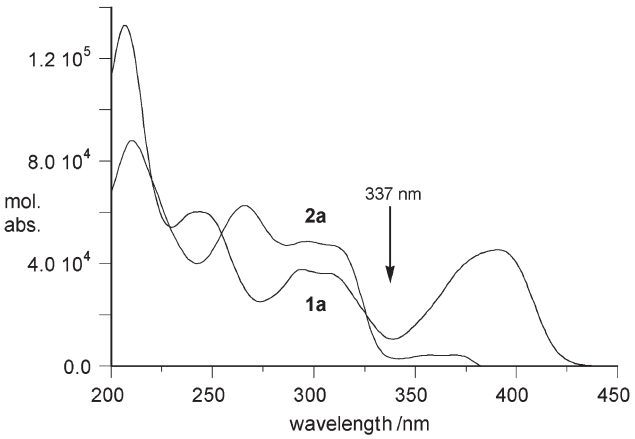

Fig. 5 UV-vis spectra for 3,4-dioctyloxyphenyl derivatives of pyrene **1a** and carbazole **2a** recorded in cyclohexane.

363 nm in **2a**. The lowest energy absorption band for **1a** has a maximum at 391 nm, which is shifted by 56 nm to the red relative to the allowed ^1L_a transition or 36 nm relative to the forbidden ^1L_b band in pyrene.[42] The absorption at 391 nm tails into the visible range, which results in a light yellow color for **1a**.

Photoconductivity

Charge carrier mobilities of pyrene **1a** and carbazole **2a** derivatives were measured by a standard TOF (time-of-flight) method[43] in 17.0 μm or 30.8 μm thick ITO-coated glass cells, respectively (for details see the Experimental section and ESI†). Natural textures of the samples were grown from the isotropic phase (see Fig. 1).

Raw data for photocurrent as a function of time were analyzed in double logarithmic plots. A typical presentation of data is shown in Fig. 6 for positive and negative photocurrents generated in the Col_h phase of pyrene **1a** at 60 °C.

The intercept of the two lines corresponding to the pre- and post-transit slopes of the photocurrent in the double

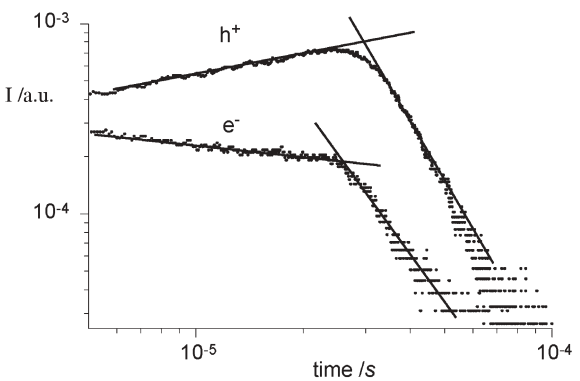

Fig. 6 Photocurrent I transient decay curves in the hexagonal columnar mesophase of pyrene **1a** at 60 °C for the positive (h^+) and negative (e^-) carriers obtained by the TOF method. Wavelength of laser pulse: 337 nm, electric field strength: 20 kV cm^{-1}, sample thickness: 17.0 μm, bias: 34.0 V. The intercept of the two lines shows the transit time t_T. The stripe pattern of the graph results from digitalization of the signal.

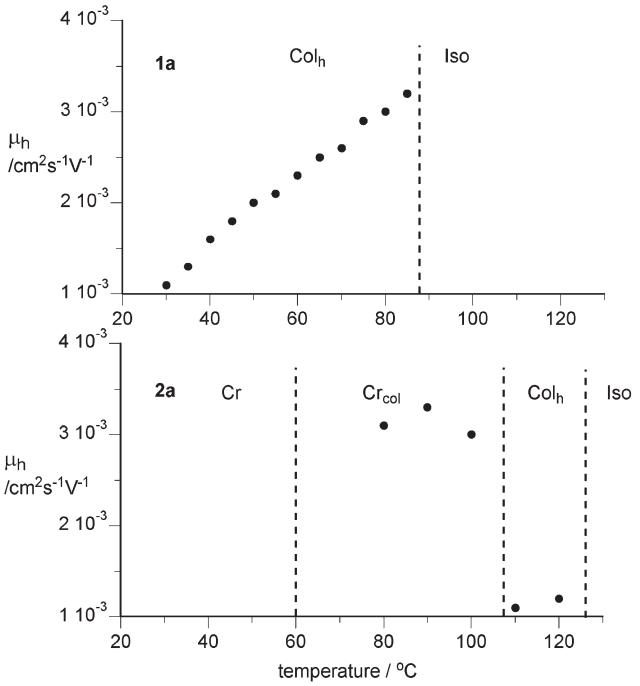

Fig. 7 The temperature dependence of positive carrier mobilities obtained by the TOF method for pyrene **1a** (top) and carbazole **2a** (bottom). Electric field strength: 30 kV cm^{-1}.

logarithmic plot gave the transit time t_T,[44] which was used to calculate the charge carrier mobility μ according to eqn (2) (l is the sample thickness and V is the applied voltage).

$$\mu = l^2/t_T V \quad (2)$$

Photocurrent generation was investigated over a range of temperatures and results for positive charge carriers (holes) mobility as a function of temperature are shown in Fig. 7. The full tabularized data are listed in the ESI.†

In general, the charge mobility recorded within the same phase was decreasing with decreasing temperature, and was bias-independent, which is characteristic for liquid crystalline semiconductors. Analysis showed that the charge transport in columnar mesophases of pyrene **1a** and carbazole **2a** derivatives and also in the crystalline columnar phase Cr_{col} of **2a** was non-dispersive and the bundle of charge carriers, electrons (when the top electrode was negative) and holes (when the top electrode was positive), was moving through the sample with a constant velocity. This was indicated by the well-defined plateau on the photocurrent curves (Fig. 6). At the transit time t_T the photocurrent decay broadened, when the charge carriers arrived at the bottom electrode.

Positive charge (hole) mobilities in unaligned samples of both compounds were found to be on the order of 10^{-3} cm^2 V^{-1} s^{-1}, which is typical for many other discotic mesogens in the Col_h phase.[45,46] Measurements of the negative charge mobility for pyrene **1a** at several temperatures gave values that are close to the hole mobility. Such ambipolar charge transport has been observed for other well-purified[46–48] discogens including phthalocyanines[17] and triphenylenes,[48] and is consistent with a hopping transport mechanism.[49] In

contrast, measurements of negative photocurrents in both Col_h and Cr_{col} phases of carbazole **2a** were less unequivocal, and precise values for charge mobility could not be obtained. This is presumably due to the presence of small ionic impurities which obscure the analysis and determination of μ_e[47] especially in a thick cell (30.8 μm).[46]

Upon cooling from the Col_h phase, carbazole **2a** shows an abrupt increase of charge mobility by a factor of 3 at the phase transition to the Cr_{col} phase (Fig. 7). This is consistent with a transition to a more organized phase and better intermolecular contact within the columns. Support for this is provided by XRD results, which show a decrease of the mean core–core distance by 0.2 Å upon Col_h to Cr_{col} transition (Fig. 4). Measurements conducted at 30 °C for the crystalline phase of carbazole **2a** showed completely dispersive charge transport. This can be interpreted as a disruption in hexagonally arranged transport tunnels in the Cr_{col} phase by creating the grain boundaries during crystallization.[2] Consequently, charge carriers were deeply trapped before they were able to reach the counter electrode.

The behavior of pyrene **1a** is different from that of **2a**, and the charge mobility follows a monotonous decrease with decreasing temperature (Fig. 7). Pyrene **1a** supercools to room temperature forming a rigid glass (*vide supra*) with structural features of the preceding Col_h phase and without disruption of the charge transport tunnels. An Arrhenius plot of the positive charge mobility data gave an activation energy for **1a** of 0.10 ± 0.01 eV (Fig. 8). This low E_a value and weak temperature dependence of μ_h are consistent with the charge hopping mechanism and intracolumn charge transport.[7,50] Ionic charge transport shows larger temperature dependence and E_a in the range of 0.2–0.4 eV.[48]

The observed charge mobilities in **1a** and **2a** are comparable to those obtained for typical materials[20] with natural homeotropic alignment such as triphenylenes[51] in which large homeotropic domains are formed by slow cooling from the isotropic phase. The alignment of samples by slow cooling in a magnetic field does not significantly affect the photoconductivity results.[3] Higher charge mobilities close to 1 $cm^2\ V^{-1}\ s^{-1}$ are observed for large planar systems[52] such as hexabenzocoronenes and superphenalenes,[19] and other highly ordered systems.[2] Similarly, high electron mobilities on the order of 0.1 $cm^2\ V^{-1}\ s^{-1}$ have been reported for large π-electron deficient discotics.[53]

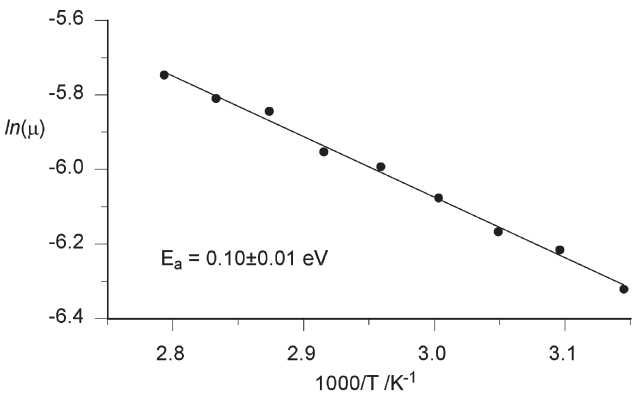

Fig. 8 Arrhenius plot for positive charge mobility in **1a** in the temperature range of 45 °C–85 °C.

Conclusions

TOF results indicate that the charge transport in pyrene **1a** is ambipolar, while the carbazole derivative **2a** behaves as a p-type semiconductor. Positive (hole) carrier mobilities are on the order of $10^{-3}\ cm^2\ V^{-1}\ s^{-1}$ and are typical for a hexagonal mesophase. The formation of an ordered glass phase rather than a crystal lattice in **1a** results in a broad range Arrhenius-type behavior of charge mobilities. Phase behavior of **1a** and **2a** allows for the formation rigid phases (frozen Col_h and Cr_{col}) with charge mobilities typical for a fluid mesogen.

Experimental

All NMR spectra were obtained at 300 MHz (^1H) and 75 MHz (^{13}C) in $CDCl_3$. Chemical shifts were referenced to TMS (^1H) or solvent (^{13}C). IR spectra were recorded for neat samples (liquid or microcrystalline) on NaCl plates. Elemental analysis was provided by Atlantic Microlabs.

Optical microscopy was performed using a PZO Biolar microscope equipped with an HS1 Instec hot stage. Phase transition temperatures were reported as onset of the peak and were obtained from a TA Instruments DSC 2920. Samples were heated and cooled with the temperature rate of 10 °C min^{-1}. UV spectra were recorded in cyclohexane and molar absorption was obtained from a Beer's law plot of 4–5 concentrations. XRD measurements were carried out using a Rigaku RINT2000 X-ray diffractometer with a homemade heater.

The charge carrier mobilities of liquid crystals were measured by the TOF (time-of-flight) method[43] using a nitrogen gas laser (Nippon Laser, λ = 337 nm) and a polarizing microscope with a hot stage. The cells were mounted on a commercially available hot stage and electric bias was applied by a stabilized DC power supply. Depending on the polarity of the applied field, positive (holes) or negative (electrons) charge carriers were moving through the sample, causing displacement photocurrent, which was detected on a digital oscilloscope with a homemade preamplifier. A schematic diagram of the experimental apparatus is shown in Fig. 9.

The cell thickness was 17.0 μm for pyrene derivative **1a** and 30.8 μm for carbazole derivative **2a**. The cells were filled with isotropic material by capillary forces. The material was

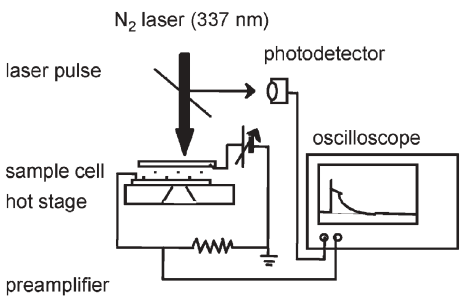

Fig. 9 Schematic diagram of the experimental apparatus (TOF method).

slowly cooled to a discotic hexagonal phase and stabilized. No magnetic field was used for sample alignment. Polarized optical microscopy showed a highly birefringent texture for **1a** practically with no homeotropic domains, while the texture of the carbazole derivative **2a** exhibited large homeotropic domains with discotic columnar axes perpendicular to the electrodes.

1,3,6,8-Tetraarylcarbazole (2). General procedure

A mixture of 1,3,6,8-tetrabromocarbazole[32] (**4**, 482 mg, 1 mmol), appropriate boronic ester **5** (4.4 mmol), $(Ph_3P)_4Pd$ (0.2 mmol), 2 M aqueous solution of Na_2CO_3 (4 mL), EtOH (4 mL), and toluene (40 mL) was refluxed for 24–72 h under N_2 until a single major product was observed by TLC. The reaction mixture was cooled, Et_2O was added, and the organic layer was separated and dried (Na_2SO_4). The solvent was evaporated and the crude product was passed through a silica gel plug with hexanes–CH_2Cl_2 (2 : 1 ratio). The product was isolated by column chromatography (pure hexanes followed by increasing ratio of hexanes–CH_2Cl_2) followed by recrystallization from a hexanes–ethanol mixture.

1,3,6,8-Tetrakis(3,4-dioctyloxyphenyl)carbazole (2a). Cr 61 (3 kJ mol^{-1}) Cr_{col} 109 (24 kJ mol^{-1}) Col_h 126 (20 kJ mol^{-1}) Iso; ^{1}H NMR δ 0.78–0.85 (m, 24H), 1.22–1.44 (m, 80H), 1.73–1.85 (m, 16H), 3.95–4.07 (m, 16H), 6.92 (d, J = 1.6 Hz, 2H), 6.95 (s, 2H), 7.15–7.22 (m, 8H), 7.55 (d, J = 1.6 Hz, 2H), 8.16 (d, J = 1.5 Hz, 2H), 8.44 (s, 1H); IR 3438 (NH), 1514 (C=C) 1248 (C–O–C) cm^{-1}; UV-vis λ_{max} (log ε): 209 (4.99), 267 (4.91), 358 (3.83), 368 (3.83). Anal. Calcd for $C_{100}H_{153}NO_8$: C, 80.22; H, 10.30; N, 0.94. Found: C, 80.09; H, 10. 32; N, 0.94%.

1,3,6,8-Tetrakis(4-octyloxyphenyl)carbazole (2b). Cr_1 104 (6 kJ mol^{-1}) Cr_2 114 (38 kJ mol^{-1}) Iso; ^{1}H NMR δ 0.83 (t, J = 6.5 Hz, 12H), 1.19–1.45 (m, 40H), 1.71–1.81 (m, 8H), 3.96 (t, J = 6.5 Hz, 4H), 3.97 (t, J = 6.5 Hz, 4H), 6.94 (d, J = 8.7 Hz, 4H), 6.99 (d, J = 8.7 Hz, 4H), 7.54 (s, 2H), 7.55 (d, J = 8.3 Hz, 4H), 7.60 (d, J = 8.7 Hz, 4H), 8.18 (s, 2H), 8.35 (s, 1H); ^{13}C NMR δ 14.1, 22.7, 26.1, 29.27, 29.32, 29.36, 29.40, 31.8, 68.1, 114.8, 115.3, 117.1, 124.7, 125.0, 125.1, 128.3, 129.2, 131.0, 133.4, 134.4, 136.8, 158.3, 158.7; IR 3479 (NH), 1511 (C=C) 1250 (C–O–C) cm^{-1}. Anal. Calcd for $C_{68}H_{89}NO_4$: C, 82.96; H, 9.11; N, 1.42. Found: C, 82.78; H, 9.11; N, 1.42%.

1,3,6,8-Tetrakis(3,5-dioctyloxyphenyl)carbazole (2c). Liquid: ^{1}H NMR δ 0.86 (t, J = 6.4 Hz, 12H), 0.89 (t, J = 6.5 Hz, 12H), (m, 24H), 1.30–1.50 (m, 80H), 1.74–1.85 (m, 16H), 3.98 (t, J = 6.6 Hz, 8H), 4.05 (t, J = 6.5 Hz, 8H), 6.48 (t, J = 2.1 Hz, 2H), 6.51 (t, J = 2.1 Hz, 2H), 6.81 (d, J = 2.2 Hz, 4H), 6.98 (d, J = 2.2 Hz, 4H), 7.71 (d, J = 1.6 Hz, 2H), 8.32 (d, J = 1.4 Hz, 2H), 8.66 (s, 1H); IR 3459 (NH), 1590 (C=C) 1166 (C–O–C) cm^{-1}. Anal. Calcd for $C_{100}H_{153}NO_8$: C, 80.22; H, 10.30; N, 0.94. Found: C, 80.37; H, 10.37; N, 0.90%.

Acknowledgements

This project was supported by NSF grants (CHE-9528029 and CHE-0096827). We thank Prof. Paul A. Heiney for valuable suggestions concerning the interpretation of the XRD results. We are also in debt to Dr Wiktor A. Piecek, a visiting NATO Fellow on leave from Military University of Technology (Warsaw, Poland), for his technical assistance.

References

1 D. Adam, F. Closs, T. Frey, D. Funhoff, D. Haarer, H. Ringsdorf, P. Schuhmacher and K. Siemensmeyer, *Phys. Rev. Lett.*, 1993, **70**, 457–460.
2 D. Adam, P. Schuhmacher, J. Simmerer, L. Haeussling, K. Siemensmeyer, K. H. Etzbach, H. Ringsdorf and D. Haarer, *Nature*, 1994, **371**, 141–143.
3 N. Boden, R. J. Bushby, J. Clements, B. Movaghar, K. J. Fonobsn and T. Kreouzis, *Phys. Rev. B*, 1995, **52**, 13274–13280.
4 D. Adam, W. Roemhildt and D. Haarer, *Jpn. J. Appl. Phys.*, 1996, **35**, 1826–1831.
5 A. Ochse, A. Kettner, J. Kopitzke, J. H. Wendorff and H. Bassler, *Phys. Chem. Chem. Phys.*, 1999, **1**, 1757–1760.
6 S. Chandrasekhar and S. K. Prasad, *Contemp. Phys.*, 1999, **40**, 237–245.
7 T. Kreouzis, K. J. Donovan, N. Boden, R. J. Bushby, O. R. Lozman and Q. Liu, *J. Chem. Phys.*, 2001, **114**, 1797–1802.
8 K. J. Donovan, T. Kreouzis, K. Scott, J. C. Bunning, R. J. Bushby, N. Boden, O. R. Lozman and B. Movaghar, *Mol. Cryst. Liq. Cryst.*, 2003, **396**, 91–112.
9 S. Chandrasekhar, in *Handbook of Liquid Crystals*, ed. D. Demus, J. W. Goodby, G. W. Gray, H.-W. Spiess and V. Vill, Wiley-VCH, New York, 1998, vol. 2B, pp. 749–780; N. Boden and B. Movaghar, in *Handbook of Liquid Crystals*, ed. D. Demus, J. W. Goodby, G. W. Gray, H.-W. Spiess and V. Vill, Wiley-VCH, New York, 1998, vol. 2B, pp. 781–798; R. J. Bushby and O. R. Lozman, *Curr. Opin. Colloid Interface Sci.*, 2002, **7**, 343–354.
10 S. Kumar, *Chem. Soc. Rev.*, 2006, **35**, 83–109.
11 I. H. Stapff, V. Stumpflen, J. H. Wendorff, D. B. Spohn and D. Mobius, *Liq. Cryst.*, 1997, **23**, 613–617; I. Seguy, P. Jolinat, P. Destruel, J. Farenc, R. Mamy, H. Bock, J. Ip and T. P. Nguyen, *J. Appl. Phys.*, 2001, **89**, 5442–5448.
12 L. Schmidt-Mende, A. Fechtenkotter, K. Müllen, E. Moons, R. H. Friend and J. D. Mackenzie, *Science*, 2001, **293**, 1119–1122.
13 A. M. van de Craats, N. Stutzmann, O. Bunk, M. M. Nielsen, M. Watson, K. Mullen, H. D. Chanzy, H. Sirringhaus and R. H. Friend, *Adv. Mater.*, 2003, **15**, 495–499.
14 I. McCulloch, W. Zhang, M. Heeney, C. Bailey, M. Giles, D. Graham, M. Shkunov, D. Sparrowe and M. Tierney, *J. Mater. Chem.*, 2003, **13**, 2436–2444.
15 C. W. Struijk, A. B. Sieval, J. E. J. Dakhorst, M. van Dijk, P. Kimkes, R. B. M. Koehorst, H. Donker, T. J. Schaafsma, S. J. Picken, A. M. van de Craats, J. M. Warman, H. Zuilhof and E. J. R. Sudholter, *J. Am. Chem. Soc.*, 2000, **122**, 11057–11066.
16 H. Fujikake, T. Murashige, M. Sugibayashi and K. Ohta, *Appl. Phys. Lett.*, 2004, **85**, 3474–3476.
17 H. Iino, J. Hanna, R. J. Bushby, B. Movaghar, B. J. Whitaker and M. J. Cook, *Appl. Phys. Lett.*, 2005, **87**, 132102.
18 A. M. van de Craats, J. M. Warman, A. Fechtenkotter, J. D. Brand, M. A. Harbison and K. Mullen, *Adv. Mater.*, 1999, **11**, 1469–1472.
19 M. G. Debije, J. Piris, M. P. de Haas, J. M. Warman, Z. Tomovic, C. D. Simpson, M. D. Watson and K. Muellen, *J. Am. Chem. Soc.*, 2004, **126**, 4641–4645.
20 R. J. Bushby and O. R. Lozman, *Curr. Opin. Solid State Mater. Sci.*, 2003, **6**, 569–578.
21 S. F. Nelson, Y.-Y. Lin, D. J. Gundlach and T. N. Jackson, *Appl. Phys. Lett.*, 1998, **72**, 1854–1856; F. Granier, G. Horowitz, X. Peng and D. Fichou, *Adv. Mater.*, 1990, **2**, 592–594.
22 N. Karl, K.-H. Kraft, J. Marktanner, M. Munch, F. Schatz, R. Stehle and H.-M. Uhde, *J. Vac. Sci. Technol., A*, 1999, **17**, 2318–2328.
23 R. F. Chaiken and D. R. Kearns, *J. Chem. Phys.*, 1968, **49**, 2846–2850.
24 M. Tierney and D. Lubman, *Appl. Spectrosc.*, 1987, **41**, 880–886.
25 R. A. Holroyd, J. M. Preses, E. H. Boettcher and W. F. Schmidt, *J. Phys. Chem.*, 1984, **88**, 744–749.
26 R. Oshima, T. Uryu and M. Seno, *Macromolecules*, 1985, **18**, 1043–1045.

27 T. Uryu, H. Ohkawa and R. Oshima, *Macromolecules*, 1987, **20**, 712–716.
28 D. W. Kim, H. Moon, S. Y. Park and S. I. Hong, *React. Funct. Polym.*, 1999, **42**, 73–86.
29 K.-Y. Law, *Chem. Rev.*, 1993, **93**, 449–486.
30 K. J. Donovan, K. Scott, M. Somerton, J. Preece and M. Manickam, *Chem. Phys.*, 2006, **322**, 471–476.
31 M. J. Sienkowska, J. M. Farrar, F. Zhang, S. Kusuma, P. A. Heiney and P. Kaszynski, *J. Mater. Chem.*, 2007, **17**, DOI: 10.1039/b615545f.
32 K. Smith, D. M. James, A. G. Mistry, M. R. Bye and D. J. Faulkner, *Tetrahedron*, 1992, **48**, 7479–7488.
33 N. Miyaura, T. Yanagi and A. Suzuki, *Synth. Commun.*, 1981, **11**, 513–519.
34 K. Ogino, S. Iwashima, H. Inokuchi and Y. Harada, *Bull. Chem. Soc. Jpn.*, 1965, **38**, 473–477.
35 S. Chandrasekhar, B. K. Sadashiva and K. A. Suresh, *Pramana*, 1977, **9**, 471–480.
36 I. Dierking, *Textures of Liquid Crystals*, Wiley-VCH, Weinheim, 2003.
37 N. Boden, R. J. Bushby, A. N. Cammidge and P. S. Martin, *J. Mater. Chem.*, 1995, **5**, 1857–1860.
38 N. Boden, R. J. Bushby, A. N. Cammidge, A. El-Mansoury, P. S. Martin and Z. Lu, *J. Mater. Chem.*, 1999, **9**, 1391–1402.
39 B. Glüsen, A. Kettner and J. H. Wendorff, *Mol. Cryst. Liq. Cryst.*, 1997, **303**, 115–120.
40 G. R. Desiraju and A. Gavezzotti, *Acta Crystallogr., Sect. B*, 1989, **45**, 473–482; C. A. Hunter, K. R. Lawson, J. Perkins and C. J. Urch, *J. Chem. Soc., Perkin Trans. 2*, 2001, 651–669.
41 S. K. Prasad, D. S. S. Rao, S. Chandrasekhar and S. Kumar, *Mol. Cryst. Liq. Cryst.*, 2003, **396**, 121–139.
42 A. C. Benniston, A. Harriman, D. J. Lawrie and S. A. Rostron, *Eur. J. Org. Chem.*, 2004, 2272–2276.
43 E. Muller-Horsche, D. Haarer and H. Scher, *Phys. Rev. B*, 1987, **35**, 1273–1280.
44 H. Scher and E. W. Montroll, *Phys. Rev. B*, 1975, **12**, 2455–2477.
45 N. Boden and B. Movaghar, in *Handbook of Liquid Crystals*, ed. D. Demus, J. W. Goodby, G. W. Gray, H.-W. Spiess and V. Vill, Wiley-VCH, New York, 1998, vol. 2B, pp. 781–798.
46 H. Iino, Y. Takayashiki, J. Hanna, R. J. Bushby and D. Haarer, *Proc. SPIE–Int. Soc. Opt. Eng.*, 2005, **5940**, 594008.
47 H. Iino, Y. Takayashiki, J. Hanna, R. J. Bushby and D. Haarer, *Appl. Phys. Lett.*, 2005, **87**, 192105.
48 H. Iino, J. Hanna, D. Haarer and R. J. Bushby, *Jpn. J. Appl. Phys.*, 2006, **45**, 430–433.
49 N. Boden, R. J. Bushby and J. Clements, *J. Chem. Phys.*, 1993, **98**, 5920–5931; L. Lever, R. Kelsall and R. J. Bushby, *J. Comput. Electron.*, 2005, **4**, 101–104; V. Lemaur, D. A. Da Silva Filho, V. Coropceanu, M. Lehmann, Y. Geerts, J. Piris, M. G. Debije, A. M. van de Craats, K. Senthilkumar, L. D. A. Siebbeles, J. M. Warman, J.-L. Bredas and J. Cornil, *J. Am. Chem. Soc.*, 2004, **126**, 3271–3279.
50 H. Nakayama, M. Ozaki, W. F. Schmidt and K. Yoshino, *Jpn. J. Appl. Phys.*, 1999, **38**, L1038–L1041.
51 J. Simmerer, B. Glüsen, W. Paulus, A. Kettner, P. Schuhmacher, D. Adam, K. H. Etzbach, K. Siemensmeyer, J. H. Wendorff, H. Ringsdorf and D. Haarer, *Adv. Mater.*, 1996, **8**, 815–819.
52 A. M. van de Craats and J. M. Warman, *Adv. Mater.*, 2001, **13**, 130–133.
53 M. Lehmann, G. Kestemont, R. G. Aspe, C. Buess-Herman, M. H. J. Koch, M. G. Debije, J. Piris, M. P. de Haas, J. M. Warman, M. D. Watson, V. Lemaur, J. Cornil, Y. H. Geerts, R. Gearba and D. A. Ivanov, *Chem.–Eur. J.*, 2005, **11**, 3349–3362.

